IEEE Access
Multidisciplinary | Rapid Review | Open Access Journal

Received January 31, 2019, accepted February 27, 2019, date of publication March 6, 2019, date of current version March 26, 2019.

*Digital Object Identifier 10.1109/ACCESS.2019.2903350*

# Fault Overload Control Method for High-Proportion Wind Power Transmission Systems Based on Emergency Acceleration of Doubly-Fed Induction Generator

**JINXIN OUYANG, (Member, IEEE), ZHEN ZHANG, TING TANG, MINGYU PANG, MENGYANG LI, AND DI ZHENG**

State Key Laboratory of Power Transmission Equipment and System Security and New Technology, School of Electrical Engineering, Chongqing University, Chongqing 400044, China

Corresponding author: Jinxin Ouyang (jinxinoy@163.com)

This work was supported in part by the National Natural Science Foundation of China under Grant 51877018, in part by the Smart Grid Technology and Equipment Key Special Foundation of National Key Research and Development Plan under Grant 2016YFB0900600, and in part by the Technology Projects of State Grid Corporation of China under Grant 52094017000W.

**ABSTRACT** With a high proportion of wind power being transmitted through ac and dc lines, a new power grid pattern has gradually emerged. A dc inverter is prone to commutation failure, which may lead to cascading trip of ac lines for overload, resulting in serious consequences. However, existing control methods have problems of over- or under-shedding and are unsuitable for high-proportion wind power transmission systems. Accordingly, a new fault overload control method based on emergency acceleration of doubly fed induction generator (DFIG) is proposed. The fast power control capability of DFIG is fully utilized; the active power of power grid could be rapidly balanced. First, the fault characteristics of a wind power ac/dc transmission system under the fault of dc receiving-end grid are analyzed, and the power flow transfer after self-recovery from the dc commutation failure is derived. Second, by analyzing the power characteristics of DFIG, a fault overload control idea of the wind power transmission system is proposed based on emergency acceleration of DFIG. At last, the maximum controllable capacity of a wind farm is analyzed, and a fault overload control strategy of the wind power transmission system is proposed. The simulation results prove that the proposed method can rapidly reduce the output of wind farms and prevent the overload of ac lines.

**INDEX TERMS** AC/DC system, DFIG-based wind farm, power flow transfer, cascading trip, emergency power control.

## I. INTRODUCTION

Wind energy resources and load centers are reversely distributed. Wind power development generally adopts the mode of large-scale centralized development and long-distance high-voltage transmission [1]. Wind power transmission through line-commutated converter based high-voltage direct current (LCC-HVDC) has become the main method of cross-zone allocation for wind energy resources because LCC-HVDC transmission system has a large transmission capacity and long transmission distance. Thus, high-proportion wind power AC/DC transmission system has emerged [2], [3].

The inverter of LCC-HVDC is prone to commutation failure due to the voltage drop of AC bus and even causes continuous commutation failure, leading to DC block [4], [5]. DC block further triggers strong disturbance and impacts AC power grid [6], [7]. Accidents, such as the March 21 blackout in Brazil, indicate that the commutation failure or DC block could impede the active power transmission of LCC-HVDC. Then the large-scale power flow transfer causes cascading trip of the AC line due to its insufficient carrying capacity, which greatly threatens the safe and stable operation of power system [8], [9].

The associate editor coordinating the review of this manuscript and approving it for publication was Datong Liu.

The components of power grid should meet the N-1 principle. Under DC commutation failure or block, other lines should not trip due to overload [10]. Therefore, studying the problem of line overload caused by power flow transfer is necessary. By establishing a simplified model of wind power AC/DC transmission system, combined with mathematical derivation and simulation experiment, Mirsaeidi *et al.* [5] and Tu *et al.* [11] analyzed the mechanism of AC line cascading trip caused by power flow transfer. In [12], the transmission limit was increased by strengthening the AC synchronous power grid, but the construction cycle was too lengthy. In [13], a unified power flow controller was utilized to improve the power flow distribution of AC power grid. However, the operation was too costly. The cascading failure caused by power flow transfer can be avoided through DC back-to-back asynchronous interconnection, but the active power impact causes the frequency of sending-end grid to increase. The inertia of sending-end grid is considerably reduced due to the application of large-scale wind turbines, the frequency changes cannot be suppressed in time [14]. In [15], the rectifier controller of LCC-HVDC was modified to aid in the frequency control of sending-end grid. However, the LCC-HVDC rectifier was out of control under DC block.

The above researches suppress power flow transfer by improving the tolerance and accommodation capacity of transmission system. However, reducing the active power of sending-end grid is the key to solving power flow transfer. The method of generator-shedding was adopted in [16], and Chen *et al.* [17] proposed a scheme of preferentially shedding the wind turbines after considering the volatility of wind power. However, the method of generator-shedding has problems of under- or over-shedding, increases the startup and shutdown times of thermal power units, even deteriorates the operating conditions of wind turbines. DFIG has fast and flexible power control capability, but has not been applied to suppress power flow transfer. DFIG generally operates at medium and low wind speeds. Wind energy can be rapidly stored in the kinetic energy of rotor by actively increasing the rotor speed, then the active power of wind turbines can be reduced [18], [19]. Accelerating the wind turbine can not only alleviate the active power imbalance of power grid but also contribute to fault recovery. Besides, power flow transfer mainly affects the backup protection of AC transmission line, and the backup protection requires much time to operate, which creates conditions for the emergency control of wind turbines.

To solve the fault overload of AC line caused by power flow transfer after the commutation failure of LCC-HVDC, a new line fault overload control method based on emergency acceleration of DFIGs is proposed with the following advantages: 1) The abundant adjustable capacity is supplied to achieve the fast power balance; 2) The under- or over-shedding is avoided; 3) The rapid recovery of electricity outage can be realized; 4) The cost of startup and shutdown of the thermal power plants is reduced.

This paper is organized as follows: Section II presents the model of wind power AC/DC transmission system, and the operating characteristics are analyzed. In Section III, the cascading failure characteristics of wind power AC/DC transmission system are analyzed, and the power flow transfer caused by DC commutation failure is derived. In Section IV, the idea of fault overload control based on emergency acceleration of DFIGs is proposed, and the maximum controllable capacity of wind farm is analyzed. In Section V, the fault overload control strategy of wind power AC/DC transmission system is proposed. In Section VI, the effectiveness of the strategy is verified through simulation.

## II. MODEL AND OPERATION CHARACTERISTICS OF WIND POWER AC/DC TRANSMISSION SYSTEMS

Large-scale centralized-developed wind farms are generally integrated through long-distance transmission systems, the proportion of wind power at the sending-end grid is high. Typically, the transmission systems have multiple terminals in the receiving-end grid, which can not only realize power cross-zone allocation through DC transmission, but also achieve the synchronous interconnection with regional power grid through AC transmission. Thus, the grid structure of high-proportion wind power AC/DC transmission has emerged, as show in Fig. 1. The wind farm mainly uses DFIG, the DC system uses LCC-HVDC transmission, and the AC system uses high-voltage AC (HVAC) transmission.

### A. MODEL AND POWER CHARACTERISTICS OF DFIG

DFIG consists of wind turbine, induction generator, and back-to-back converter. Fig. 2 illustrates the control structure of DFIG. The rotor side converter (RSC) realizes the decoupling control of DFIG stator active and reactive power by adjusting the rotor current. The grid side converter (GSC) is used to control the DC bus voltage and reactive power. The double-loop design is generally adopted by the control system of RSC. The outer loop determines the reference value of rotor current according to the reference values of electromagnetic torque and reactive power. The inner loop is the current control loop, which calculates the voltage reference value according to the reference current.

When the wind energy drives the blades of wind turbine to rotate, the mechanical power of DFIG is

$$P_{\mathrm{g}} = k_1 v^3 C_{\mathrm{p}}(\lambda) \tag{1}$$

where $k_1$ is the correlation coefficient of wind turbine, $v$ is the wind speed, $C_{\mathrm{p}}$ is the wind energy utilization coefficient, a function of tip speed ratio $\lambda$. $C_{\mathrm{p}}$ can be fitted as [20]

$$C_{\mathrm{p}} = \left(\frac{25.52}{\lambda} - 1.9932\right) e^{-\frac{12.5}{\lambda}+0.4375} \tag{2}$$

where the tip speed ratio $\lambda$ can be expressed as

$$\lambda = k_2 \omega_{\mathrm{r}} / v \tag{3}$$

where $k_2$ is the correlation coefficient of wind turbine, $\omega_{\mathrm{r}}$ is the rotor speed of DFIG.

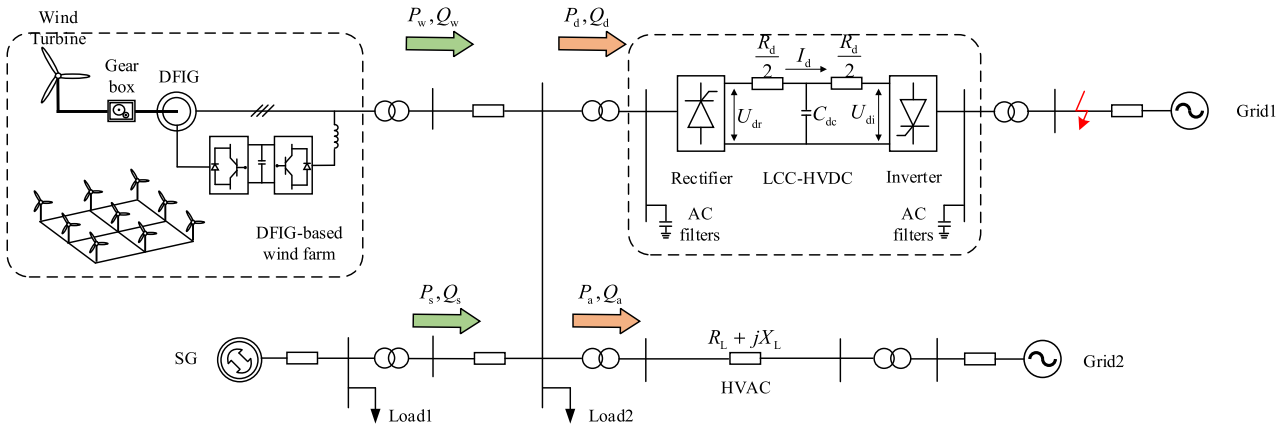


**FIGURE 1.** High-proportion wind power AC/DC transmission system.

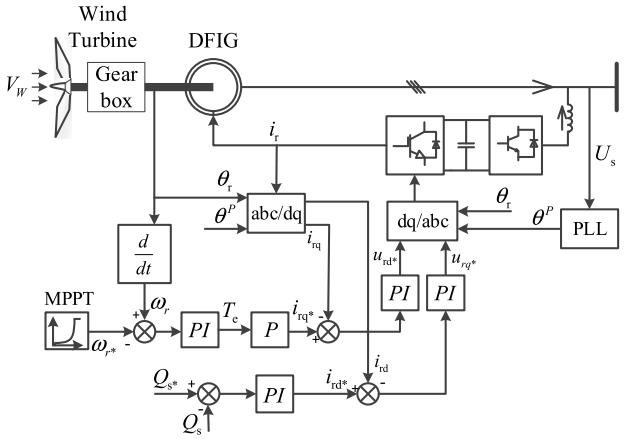


**FIGURE 2.** Control structure of DFIG.

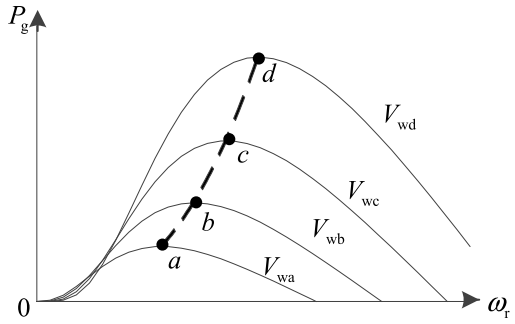


**FIGURE 3.** Power characteristics of DFIG.

To achieve maximum power point tracking (MPPT) control, the reference value of rotor speed is designated as the optimal speed $\omega_{rop}$, it can be calculated according to the real-time wind speed [21]

$$\omega_{r*} = \omega_{rop} = \lambda_{opt} v / k_2 \tag{4}$$

where the superscript "$*$" denotes the reference value, $\lambda_{opt}$ is the optimal tip speed ratio.

When rotor speed $\omega_r$ reaches the optimal speed $\omega_{rop}$, the optimal tip speed ratio $\lambda_{opt}$ and maximum utilization coefficient $C_{pmax}$ can be acquired, thus capturing the maximum wind energy.

The dashed line in Fig. 3 shows the power characteristics of DFIG according to (1), (2), and (3). Under a certain wind speed, the mechanical power of DFIG initially increases then decreases with the increase of rotor speed. When the rotor speed reaches the optimal value, the mechanical power reaches the maximum value.

### B. MODEL AND OPERATION CHARACTERISTICS OF LCC-HVDC

LCC-HVDC consists of rectifier station, inverter station, DC transmission line, and AC filter. A 12-pulse line-commutated converter is used for natural commutation in the rectifier and inverter stations. The converter is composed of thyristors, which cannot extinguish the current and require a large amount of reactive power during operation. The reactive power is mainly provided by the AC filter. In normal operations, the LCC-HVDC rectifier station adopts constant DC current and minimum firing angle control, and the inverter station adopts constant extinction angle and current deviation control. Furthermore, the rectifier and inverter stations are equipped with voltage-dependent current order limiter (VDCOL).

The DC current of LCC-HVDC $I_d$ and the DC voltage of the invertor station $U_{di}$ can be expressed as [22]

$$I_d = \frac{U_i (\cos\gamma - \cos\beta)}{\sqrt{2} T X_T} \tag{5}$$

$$U_{di} = \frac{3\sqrt{2} U_i}{\pi T} \cos\gamma - \frac{3}{\pi} X_T I_d \tag{6}$$

where $U_i$ is the converter bus voltage of inverter station, $T$ is the converter transformer ratio, $X_T$ is the leakage resistance of converter transformer, $\gamma$ is the extinction angle of inverter station, $\beta$ is the firing advance angle of inverter station.

According to (5), the extinction angle of inverter station can be expressed as

$$\gamma = \arccos\left(\frac{\sqrt{2} T I_d X_T}{U_i} + \cos\beta\right) \tag{7}$$

According to (7), $\gamma$ is related to $I_d$, $U_i$, and $\beta$. When $I_d$ increases or $U_i$ decreases, $\gamma$ decreases accordingly. Once $\gamma$ is less than the critical extinction angle $\gamma_{min}$, commutation failure occurs in the inverter, prompting the DC power to decrease or be interrupted. Therefore, when the voltage drop of the converter bus is detected, commutation failure preventive (CFPREV) control is generally activated in the inverter station to increase the firing advance angle, thereby increasing the extinction angle of the inverter station and reducing the probability of commutation failure.

## III. CASCADING FAILURE CHARACTERISTICS OF WIND POWER AC/DC TRANSMISSION SYSTEMS

When a three-phase symmetrical fault occurs at the AC side of LCC-HVDC inverter station and causes commutation failure, the DC power variation process is shown in Fig. 4. $P_d$ is the active power of LCC-HVDC transmission, the subscript "0" denotes the value before the fault, the subscript "f" denotes the steady-state value after self-recovery from the commutation failure, $t_f$ is the fault time, and $\Delta t$ is the duration of the transition process of commutation failure.

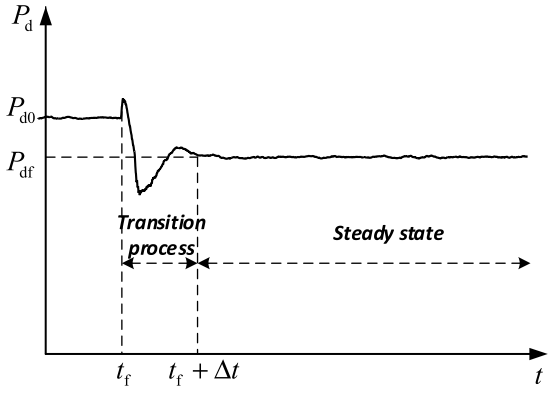


**FIGURE 4.** DC power variation process under commutation failure.

According to Fig. 4, the DC current increases suddenly during the post-fault transition process because the commutation failure of inverter is equivalent to the short circuit of DC side. Then, the DC current decreases rapidly under the effect of DC line resistance. Therefore, the DC power initially increases and then decreases. Due to the short duration of commutation failure, the DC power is gradually recovered after the inverter operates in normal commutation. Then the DC transmission system reaches a new steady state. Although the active power drop in the transition process is deep, the duration $\Delta t$ is generally 50 ms to 100 ms, which does not influence the backup protection of AC lines. In the steady state after self-recovery from commutation failure, the VDCOL of rectifier station is activated to reduce the DC current reference value because the AC bus and DC voltage of the inverter station have not been fully recovered. Thus, the DC power is maintained at a relatively low level, which can reduce the reactive power demand of inverter station and contribute to the voltage recovery of AC bus.

According to (5) and (6), the DC voltage of rectifier station under steady state after self-recovery from commutation failure can be expressed as

$$U_{drf} = \frac{\sqrt{2}U_{if}}{2T}\left[\left(\frac{R_d}{X_T} + \frac{3}{\pi}\right)\cos\gamma_f^* - \left(\frac{R_d}{X_T} - \frac{3}{\pi}\right)\cos\beta_f^*\right] \tag{8}$$

where $U_{dr}$ is the DC voltage in rectifier station, $R_d$ is the resistance of DC line.

Equation (8) shows that the rectifier DC voltage is determined by the AC bus voltage, extinction angle, and firing advance angle of the inverter station. The extinction angle is equal to the reference value $\gamma_f^*$ under the steady state of grid fault due to the constant extinction angle control adopted by the inverter station. The AC bus voltage can be obtained by measurement. Once the AC bus voltage drop is detected, the CFPREV control raises the firing advance angle. According to (7), the firing advance angle under the steady state of grid fault can be expressed as

$$\beta_f^* = \arccos\left(\cos\gamma_f^* - \frac{\sqrt{2}TI_{df}X_T}{U_{if}}\right) + \Delta\alpha \tag{9}$$

where $\Delta\alpha$ is the output of the CFPREV control, $I_{df}$ is the DC current under steady state of grid fault, it is limited by VDCOL and can be expressed as [23]

$$I_{df} = \begin{cases} I_{dh}, & U_{drf} > U_{dh} \\ I_{dl} + \dfrac{I_{dh} - I_{dl}}{U_{dh} - U_{dl}}(U_{drf} - U_{dl}), & U_{dl} \le U_{drf} \le U_{dh} \\ I_{dl}, & U_{drf} < U_{dl} \end{cases} \tag{10}$$

where $U_{dh}$, $U_{dl}$, $I_{dh}$, and $I_{dl}$ are the parameters of VDCOL.

The DC voltage and current of rectifier station can be solved with (8), (9), and (10). Therefore, compared with the active power transmitted by LCC-HVDC before fault, the active power reduction under the steady state of grid fault can be expressed as

$$\Delta P_d = U_{dr0}I_{d0} - U_{drf}I_{df} \tag{11}$$

The active power of LCC-HVDC transmission decreases, which causes the sending-end frequency to increase. However, the inertia of sending-end grid is reduced due to the application of high proportion wind power. The thermal power plants lack sufficient frequency regulation capacity. Hence, the active power output of the sending-end sources remains nearly unchanged. As a result, all active power reduced by LCC-HVDC is transferred to HVAC, and the power flow transfer is approximately equal to $\Delta P_d$, which could cause HVAC overload and further lead to a cascading trip. At the same time, the reactive power consumed by the rectifier station decreases, causing the sending-end voltage to increase. However, DFIG has the capability of high-voltage ride-through and can maintain integrated operation after fault. Therefore, its fast power control capability can be used to suppress the active power flow transfer.

## IV. FAULT OVERLOAD CONTROL IDEA BASED ON DFIG EMERGENCY ACCELERATION

For the high-proportion wind power AC/DC transmission system, under the fault on the AC side of the LCC-HVDC inverter station, reducing the sending-end active power is the key to interrupting the cascading trip of AC lines. DFIG can maintain integrated operation during the fault. Thus, reducing the active power of wind farms by emergency control can effectively suppress overload in the AC line. After commutation failure of the LCC-HVDC, DFIGs can be actively accelerated, making the tip speed ratio deviate from the optimal tip speed ratio. Hence, the wind energy utilization coefficient and active power output of DFIG can be reduced, thus avoiding the excess active power of sending-end grid. Besides, the redundant wind energy is stored as rotor kinetic energy, which can help to provide sufficient active power during fault recovery.

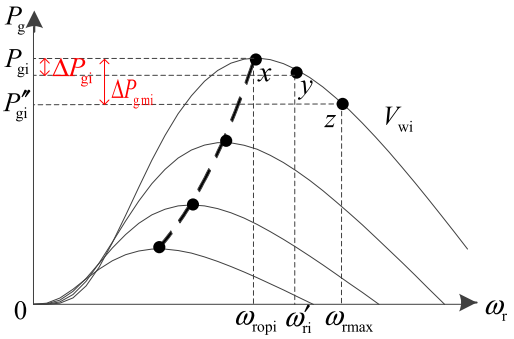


**FIGURE 5.** Power characteristics of DFIG under emergency acceleration.

When the operating wind speed is $V_{wi}$, the operating point of any DFIG under MPPT control is $x$ on the power characteristic curve, as shown in Fig. 5. $x$ is the maximum power operating point of DFIG under the wind speed of $V_{wi}$. If the DFIG rotor speed is increased to $\omega'_{ri}$, thus making the DFIG operate at point $y$ correspondingly, the mechanical power of DFIG can be reduced by $\Delta P_{gi}$. With a further increase in rotor speed, the mechanical power of DFIG decreases continuously. However, to avoid rotor over-speeding, the maximum value of rotor acceleration should be less than the maximum allowable rotor speed $\omega_{rmax}$. Therefore, the maximum reduction of mechanical power that can be achieved by rotor acceleration is

$$\Delta P_{gmi} = P_{gi} - P''_{gi} = k_1 V_{wi}^3 (C_{pmax} - C''_p) \tag{12}$$

where

$$\begin{cases} C''_p = \left(\dfrac{25.52}{\lambda''} - 1.9932\right) e^{-\frac{12.5}{\lambda''}+0.4375} \\ \lambda'' = k_2 \omega_{rmax} / V_{wi} \end{cases} \tag{13}$$

For the entire wind farm, the maximum controllable capacity is

$$\Delta P_{wm} = \sum_{i=1}^{N} \Delta P_{gmi} \tag{14}$$

where $N$ is the number of DFIG in the wind farm and $i$ indicates the i-*th* DFIG.

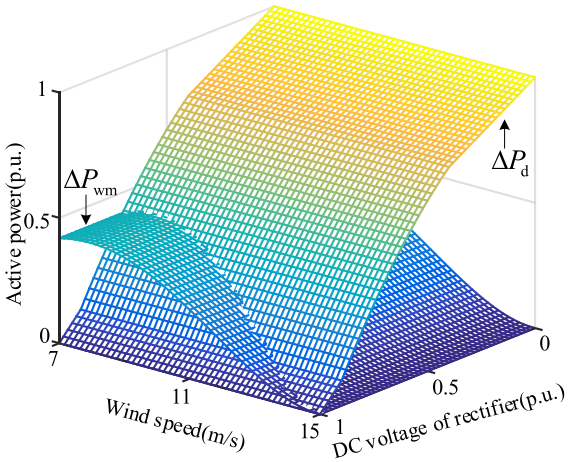


**FIGURE 6.** Relationship between power flow transfer and the maximum controllable capacity of wind farm.

The relationship between the power flow transfer and the maximum controllable capacity of wind farm can be obtained with (11) and (14), as shown in Fig. 6. The figure shows that power flow transfer $\Delta P_d$ is inversely proportional to the DC voltage of rectifier station, and the maximum controllable capacity of wind farm $\Delta P_{wm}$ decreases with the increase of wind speed. Under certain operating wind conditions and fault severity, when $\Delta P_d \leq \Delta P_{wm}$, the maximum controllable capacity of wind farm can meet the control requirements of the sending-end excessive power.

## V. FAULT OVERLOAD CONTROL STRATEGY FOR WIND POWER AC/DC TRANSMISSION SYSTEMS

When the HVAC transmission line is overloaded for a long time, the backup protection is initiated, leading to a cascading trip. Therefore, the response speed of the DFIG emergency control should be guaranteed. The outer loop of the RSC control of DFIG is generallydesigned according to the typical type II system, which has a lengthy response time. Meanwhile, the inner loop is designed according to the typical type I system, in which the bandwidth of PI controller is approximately 35 Hz with a rise time of only 10 ms [24]. Therefore, by blocking the outer loop of the RSC q-axis control and directly giving the reference value of electromagnetic torque, the fast active power control can be realized. Fig. 7 depicts the control structure.

To avoid control over-limit, the active power control amount of each DFIG is allocated according to the proportion of its maximum controllable capacity to the maximum controllable capacity of wind farm. The active power control amount of the i-*th* DFIG is

$$\Delta P_{gi} = \frac{\Delta P_{gmi}}{\Delta P_{wm}} \Delta P_d \tag{15}$$

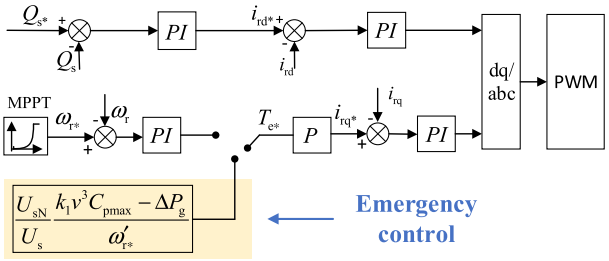


**FIGURE 7.** Control structure of RSC under emergency control.

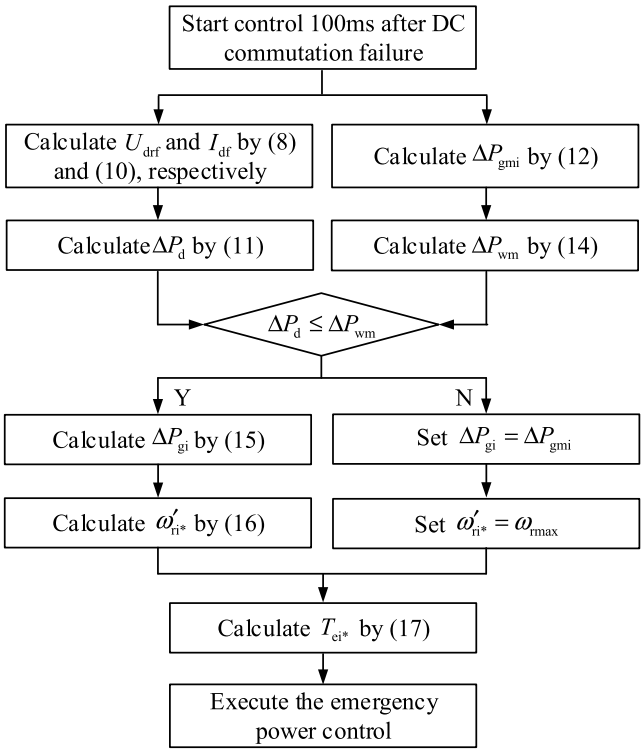


**FIGURE 8.** Fault overload control process of the wind power AC/DC transmission system.

The rotor speed reference value $\omega'_{ri*}$ of the i-*th* DFIG can be obtained using (1), (2), and (3):

$$\begin{cases} P_{gi} - \Delta P_{gi} = k_1 V_{wi}^3 C'_{pi} \\ C'_{pi} = \left(\dfrac{25.52}{\lambda'_i} - 1.9932\right) e^{-\frac{12.5}{\lambda'_i}+0.4375} \\ \lambda'_i = \dfrac{k_2 \omega'_{ri*}}{V_{wi}} \end{cases} \tag{16}$$

Thus, the electromagnetic torque reference value of the i-*th* DFIG can be expressed as

$$T_{ei*} = \frac{U_{sN}}{U_s} \frac{P_{gi} - \Delta P_{gi}}{\omega'_{ri*}} = \frac{U_{sN}}{U_s} \frac{k_1 V_{wi}^3 C_{pmax} - \Delta P_{gi}}{\omega'_{ri*}} \tag{17}$$

where $U_s$ is the RMS value of DFIG terminal voltage and $U_{sN}$ is the rated value of DFIG terminal voltage.

Fig. 8 shows the process of fault overload control. Considering the communication time and fault detect time, the control is started 100 ms after the LCC-HVDC commutation failure. First, according to the operating wind speed of each DFIG, the maximum controllable capacity of wind farm $\Delta P_{wm}$ is calculated using (12) and (14). Second, according to the AC bus voltage $U_{if}$, extinction angle $\gamma_f^*$, and firing advance angle $\beta_f^*$ of the inverter station, the DC voltage and DC current of the rectifier are calculated using (8) and (10). Then the power flow transfer under the steady state of grid fault is calculated using (11).

Furthermore, $\Delta P_d$ is compared with $\Delta P_{wm}$. When $\Delta P_d \le \Delta P_{wm}$, the active power control amount $\Delta P_{gi}$ and rotor speed reference value $\omega'_{ri*}$ are calculated by (15) and (16), respectively. When $\Delta P_d > \Delta P_{wm}$, $\Delta P_{gi} = \Delta P_{gmi}$ and $\omega'_{ri*} = \omega_{rmax}$.

The electromagnetic torque reference value of each DFIG is calculated according to (17), then directly designated to the inner loop of the RSC q-axis control. The active power output of wind farm can be adjusted rapidly through this method. The power flow transfer can be suppressed, and the cascading failure caused by the overload of AC lines can be avoided.

## VI. SIMULATION

The high-proportion wind power AC/DC transmission system shown in Fig. 1 is built in Matlab/Simulink. The rated capacity of wind farm is 1800 MW, the wind farm consists of 1,200 DFIGs (1.5 MW), they are equivalent to a DFIG by capacity weighting. The rated capacity of the thermal power plant is 1600 MW (5*320 MW). The rated voltage and capacity of the LCC-HVDC are 540 kV and 500 MW, respectively. The rated voltage of HVAC is 220 kV. The loads in the sending-end grid are simulated with constant impedance model, their total capacity is 400 MW. The detailed simulation parameters are presented in the Appendix.

In normal operation, the wind speed of each DFIG in the wind farm is 11 m/s, and the thermal power plant is dispatched to generate 640 MW (2*320 MW). Fig. 9 presents the system operation status. The active power generated by wind farm is approximately 0.36 p.u. (the reference power used in the simulation is 2,000 MVA). The active power from the thermal power plant is approximately 0.32 p.u.. The active power transmitted by HVAC is approximately 0.16 p.u.. The active power transmitted by LCC-HVDC is approximately 0.25 p.u.. The active power consumed by loads is 0.2 p.u.. Therefore, the losses of the transmission lines, the transformers, and the rectifier station is 0.07 p.u. in total. The extinction angle of inverter is maintained around the reference value of 18°.

At 4 s, a three-phase symmetrical short-circuit fault occurs on the AC side of the LCC-HVDC inverter station. The fault lasts for 500 ms, and the fault resistance is 25 Ω. As shown in Fig. 10(a), the AC bus voltage of inverter station drops to 0.85 p.u.. The CFPREV control is activated to raise the firing advance angle, which increases to 25° at the fault instant and maintains at approximately 4° under the steady state of grid fault, as shown in Fig. 10(b). After the fault, the extinction angle is reduced to 5°, which is lower than the critical extinction angle, leading to commutation failure of the

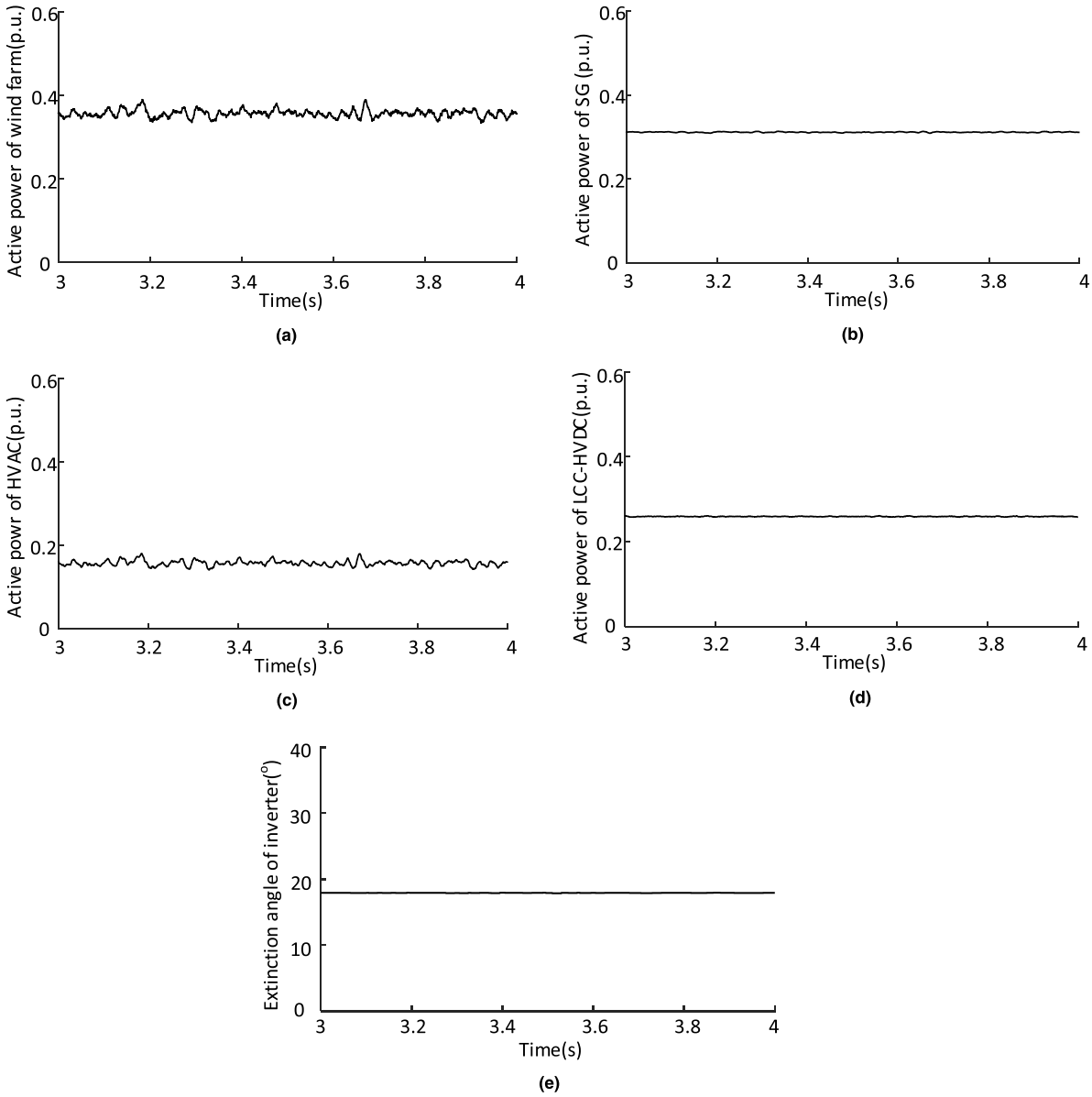


**FIGURE 9.** Normal operation characteristics of the wind power AC/DC transmission system. (a) Active power generated by wind farms. (b) Active power generated by thermal power plants. (c) Active power transmitted by HVAC. (d) Active power transmitted by LCC-HVDC. (e) Extinction angle of LCC-HVDC inverter.

inverter. After a transition process of approximately 100 ms, the extinction angle is gradually recovered to the reference value of 18°, as shown in Fig. 10(c).

According to (8), (9), and (10), the DC voltage of rectifier is calculated to reduce to 0.83 p.u. (the reference voltage is 540 kV) under the steady state of grid fault. Under VDCOL control, the DC current is limited to 0.94 p.u. (the reference current is 500 MW/540 kV). Fig. 10(d) and 10(e) show the simulated DC voltage and DC current of the rectifier, respectively. The simulation results are basically consistent with the theoretical calculation results. Under the steady state of grid fault, the active power transmitted by LCC-HVDC is reduced to approximately 0.215 p.u., as shown in Fig. 10(f). Without emergency power control, the excessive active power transfers to HVAC, causing the active power delivered by HVAC to increase by approximately 33%, from 0.15 p.u. to approximately 0.2 p.u., as shown by the red line in Fig. 11(b). As a result, the HVAC could be faced with cascading trip due to overload.

To verify the performance of the proposed emergency control, the method of generator-shedding [16] is taken for comparison. The power flow transfer is 0.055 p.u., i.e., 110 MW. Therefore, one thermal power unit is shed at 4.1 s, the active power transmitted by HVAC is shown by the yellow line in Fig. 11(b). Although the line overload is suppressed after generator-shedding, the active power transmitted by HVAC decreases too much, even the power reversal occurs, which severely influences the normal power supply.

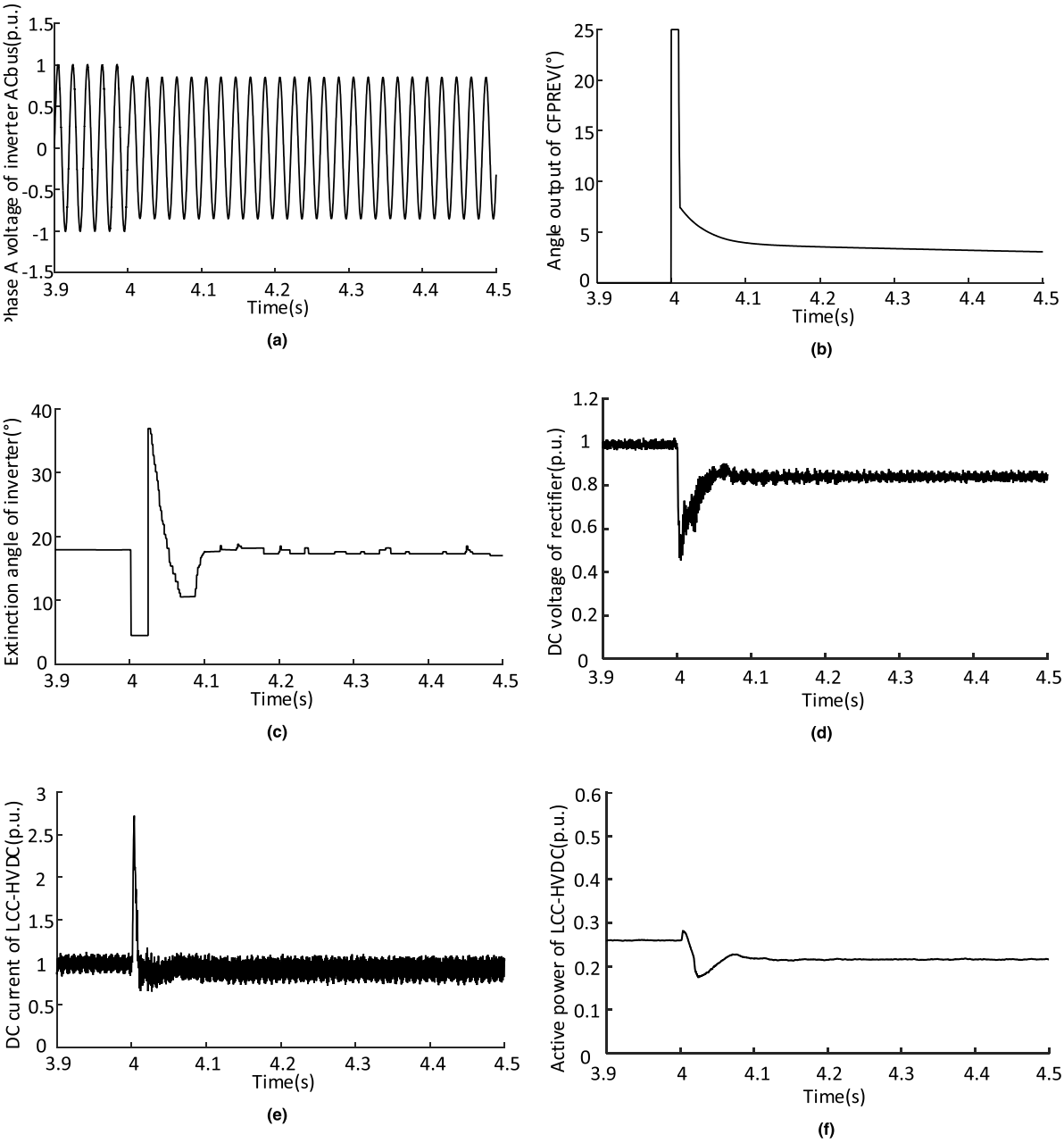


**FIGURE 10.** Operation parameters of the AC/DC system under symmetrical fault. (a) AC bus voltage of phase A at the inverter. (b) Output of CFPREV control. (c) Extinction angle of the inverter in LCC-HVDC. (d) DC voltage of the rectifier in LCC-HVDC. (e) DC current of the rectifier in LCC-HVDC. (f) Active power transmitted by LCC-HVDC.

Then the proposed emergency control is implemented. When DFIG is accelerated from the optimal speed to the maximum allowable speed, the wind energy utilization coefficient changes from 0.4382 to 0.3533. According to (14), the maximum controllable capacity of wind farm is 0.07 p.u., which is greater than the power flow transfer of 0.055 p.u.. Hence, the controllable capacity of wind farm satisfies the control demands. The wind farm emergency power control is activated 100 ms after the commutation failure. The active power control amount of wind farm is 0.055 p.u.. According to (16), the control reference value of DFIG rotor speed is 1.16 p.u.. According to (17), the corresponding electromagnetic torque reference value can be calculated as the input of the inner loop of RSC control. Under emergency control, the active power generated by wind farm decreases by approximately 0.07 p.u., as shown by the blue line in Fig. 11(a). The active power transmitted by HVAC drops by approximately 0.07 p.u. and returns to the normal operating level, as shown by the blue line in Fig. 11(b).

Compared to the method of generator-shedding, the proposed emergency power control strategy can not only effectively suppress power flow transfer, but also ensure the

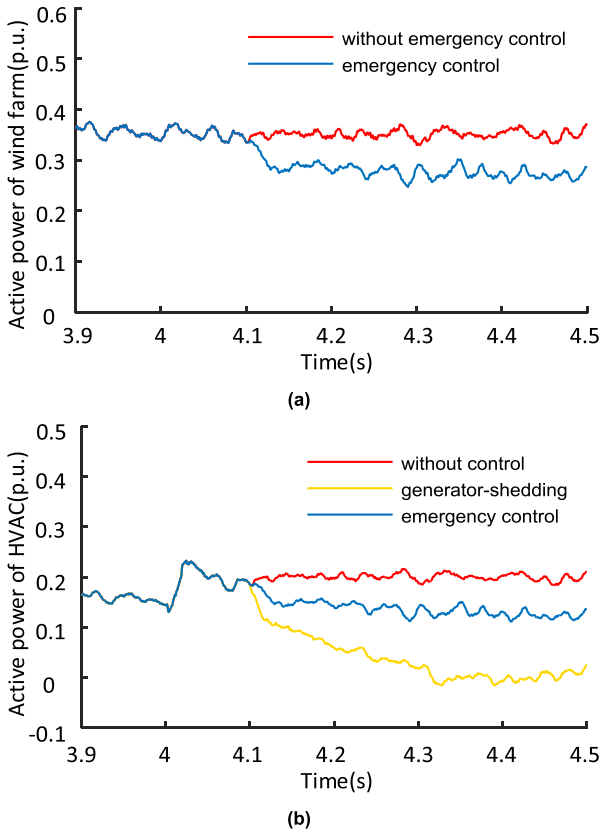


**FIGURE 11.** Comparison of simulation results. (a) Active power generated by the wind farm. (b) Active power transmitted by HVAC.

normal power supply. Besides, the duration between the start of emergency control and the achievement of control objective is only 30 ms, it is determined by the performance of the PI controller in the inner loop of RSC. Therefore, the active power transmitted by HVAC is quickly reduced, and the AC backup protection is not activated. In normal operation, the active power transmitted by HVAC is 0.15 p.u., it changes to 0.135 p.u. under emergency control, so the control error is 10%. Compared to the risk of over-shedding, the control error is acceptable.

## VII. CONCLUSION

A high-proportion wind power AC/DC transmission system is prone to DC power transmission blocking under receiving-end faults. The power flow transfer could cause HVAC overload and cascading trip. From the perspective of reducing the active power of wind farms, a new idea to rapidly reduce the sending-end active power and suppress HVAC overload through DFIG emergency acceleration is proposed. The active power control amount is allocated according to the control capability of each DFIG, and the rotor speed is adjusted accordingly. Meanwhile, the response speed of the emergency power control is improved by modifying the controller. The proposed control method can be implemented easily. The fast power control capability of DFIG is fully utilized, the safety and stability level of power system is improved, and the startup and shutdown times of thermal power plants are reduced, thus improving the energy utilization efficiency and economy. This method is suitable for the operation control of complex power systems with large-scale wind power and DC.

## APPENDIX

### A. PARAMETERS OF DFIG

rated capacity: 1.5 MW;
stator voltage: 575V;
rotor voltage: 1975 V;
DC bus voltage: 1150 V;
stator resistance: 0.0071 p.u.;
rotor resistance: 0.005 p.u.,;
stator leakage inductance: 0.1714 p.u.;
rotor leakage inductance: 0.1563 p.u.;
magnetizing inductance: 2.9 p.u.;
wind turbine correlation coefficient: $k_1$=1014.3, $k_2$=78.75.

### B. PARAMETERS OF LCC-HVDC

converter transformer ratio:
rectifier station: 486 kV/200 kV;
inverter station: 331.2 kV/200 kV;
converter transformer leakage inductance: 0.24 p.u.;
DC line length: 300 km;
DC line resistance: 0.015 Ω/km;
VDCOL parameters:
$U_{dh} = 0.9$p.u., $U_{dl} = 0.4$p.u., $I_{dh} = 1$p.u., $I_{dl} = 0.55$p.u..

### C. PARAMETERS OF HVAC

line length: 150 km;
line resistance: 0.115 Ω/km;
line inductance: $2.05 \times 10^{-3}$H/km;
Load1=200 MW; Load2=200 MW.

## REFERENCES

[1] S. Dong, Y. Chi, and Y. Li, "Active voltage feedback control for hybrid multiterminal HVDC system adopting improved synchronverters," *IEEE Trans. Power Del.*, vol. 31, no. 2, pp. 445–455, Apr. 2016.

[2] A. Yogarathinam, J. Kaur, and N. R. Chaudhuri, "Impact of inertia and effective short circuit ratio on control of frequency in weak grids interfacing LCC-HVDC and DFIG-based wind farms," *IEEE Trans. Power Del.*, vol. 32, no. 4, pp. 2040–2051, Aug. 2017.

[3] C. Liu, Y. Zhao, G. Li, and U. D. Annakkage, "Design of LCC HVDC wide-area emergency power support control based on adaptive dynamic surface control," *IET Gener., Transmiss. Distrib.*, vol. 11, no. 13, pp. 3236–3245, Sep. 2017.

[4] Z. Wei, Y. Yuan, X. Lei, H. Wang, G. Sun, and Y. Sun, "Direct-current predictive control strategy for inhibiting commutation failure in HVDC converter," *IEEE Trans. Power Syst.*, vol. 29, no. 5, pp. 2409–2417, Sep. 2014.

[5] S. Mirsaeidi, X. Dong, D. Tzelepis, D. M. Said, A. Dysko, and C. Booth, "A predictive control strategy for mitigation of commutation failure in LCC-Based HVDC systems," *IEEE Trans. Power Electron.*, vol. 34, no. 1, pp. 160–172, Jan. 2018.

[6] P. Wu, S. Xu, and B. Chao, "Research of weak sending-end coupling characteristics for bundled wind-thermal power transmission of UHVDC project," *Electr. Power Automat. Equip.*, vol. 36, no. 1, pp. 60–66, Jan. 2016.

[7] C. Zheng, S. Ma, X. Shen, and D. Liu, "Definition, connotation and form of strong HVDC and weak AC and countermeasures for stable operation of hybrid power grid," *Power Syst. Technol.*, vol. 41, no. 8, pp. 2491–2498, Feb. 2017.
[8] C.-J. Chou, Y.-K. Wu, G.-Y. Han, and C.-Y. Lee, "Comparative evaluation of the HVDC and HVAC links integrated in a large offshore wind farm—An actual case study in Taiwan," *IEEE Trans. Ind. Appl.*, vol. 48, no. 5, pp. 1639–1648, Sep./Oct. 2012.
[9] M. H. Athari and Z. Wang, "Impacts of wind power uncertainty on grid vulnerability to cascading overload failures," *IEEE Trans. Sustain. Energy*, vol. 9, no. 1, pp. 128–137, Jan. 2018.
[10] *Guide on Security and Stability for Power System*. Beijing, China: China Electric Power Press, 2001.
[11] J. Tu, J. Zhang, J. Wang, J. He, and W. Lin, "Mechanism analysis on the sending-side instability caused by the receiving-side contingencies of large-scale HVDC asynchronous interconnected power systems," *Proc. CSEE*, vol. 35, no. 21, pp. 5492–5499, Nov. 2015.
[12] H. Jingbo, L. Mingjie, Y. Jun, C. Qing, X. Tao, and Y. Zhao, "Research on dynamic characteristics and countermeasures of AC-DC hybrid power system with large scale HVDC transmission," in *Proc. IEEE Int. Confer. Power Syst. Technol.*, Oct. 2014, pp. 799–805.
[13] J. Li, F. Liu, Z. Li, S. Mei, and G. He, "Impacts and benefits of UPFC to wind power integration in unit commitment," *Renew. Energy*, vol. 116, pp. 570–583, Feb. 2018.
[14] B. Zhou, C. Hong, and X. Jin, "Study of backbone structure change from synchronous to asynchronous in China Southern Power Grid," *Proc. CSEE*, vol. 36, no. 8, pp. 2084–2092, 2016.
[15] R. Li, S. Bozhko, and G. Asher, "Frequency control design for offshore wind farm grid with LCC-HVDC link connection," *IEEE Trans. Power Electron.*, vol. 23, no. 3, pp. 1085–1092, May 2008.
[16] Z. Song, Y. Lin, C. Liu, Z. Ma, and L. Ding, "Review on over-frequency generator tripping for frequency stability control," in *Proc. IEEE Power Energy Eng. Conf.*, Oct. 2016, pp. 2240–2243.
[17] S. Chen, L. Zhu, J. Ding, Y. Song, and Y. Quan, "Impact of grid-connected wind farms on high frequency generator tripping in isolated power grid," *Power Syst. Technol.*, vol. 36, no. 1, pp. 58–64, Jan. 2012.
[18] L.-R. Chang-Chien, W.-T. Lin, and Y.-C. Yin, "Enhancing frequency response control by DFIGs in the high wind penetrated power systems," *IEEE Trans. Power Syst.*, vol. 26, no. 2, pp. 710–718, May 2011.
[19] Z. Zhou, C. Wang, L. Guo, W. Xu, and Y. Zhang, "Output power curtailment control of variable-speed variable-pitch wind turbine generator at all wind speed regions," *Proc. CSEE*, vol. 35, no. 8, pp. 1837–1844, Apr. 2015.
[20] J. F. Conroy and R. Watson, "Low-voltage ride-through of a full converter wind turbine with permanent magnet generator," *IET Renew. Power Gener.*, vol. 1, no. 3, pp. 182–189, Sep. 2007.
[21] J. Ouyang, T. Tang, Y. Diao, M. Li, and J. Yao, "Control method of doubly fed wind turbine for wind speed variation based on dynamic constraints of reactive power," *IET Renew. Power Gener.*, vol. 12, no. 9, pp. 973–980, Jul. 2018.
[22] W. Zhao, *HVDC Transmission Technology*. Beijing, China: Electric Power Press, 2011.
[23] Z. Xu, *Dynamic Behavior Analysis of AC/DC Power System*. Beijing, China: Machinery Industry Press, 2004.
[24] D. Xie, Z. Xu, L. Yang, J. Ostergaard, Y. Xue, and K. Wong, "A comprehensive LVRT control strategy for DFIG wind turbines with enhanced reactive power support," *IEEE Trans. Power Syst.*, vol. 28, no. 3, pp. 3302–3310, Aug. 2013.

Authors' photographs and biographies not available at the time of publication.